RSC Advances

PAPER

View Article Online
View Journal | View Issue

Cite this: *RSC Adv.*, 2020, **10**, 17862

Nitrogen-doped RuS_2 nanoparticles containing *in situ* reduced Ru as an efficient electrocatalyst for hydrogen evolution†

Yan Xu,[a] Xiaoping Gao,*[b] Jingyan Zhang[c] and Daqiang Gao[c]

The production of hydrogen *via* water electrolysis brings hope for the realization of hydrogen economy, but there is still a lack of highly efficient and appropriate electrocatalysts for the generation of hydrogen in practical applications. In particular, reasonable construction and feasible preparation strategies are the essential requirements for excellent electrocatalysts. Herein, the heterostructures of N-RuS_2/Ru nanoparticles were designed by annealing the RuS_2 nanoparticles in ammonia. By introducing a nitrogen dopant and single-phase Ru metal simultaneously, high-efficiency electrocatalytic performance for hydrogen evolution reaction (HER) was implemented, where the electrocatalyst of N-RuS_2/Ru exhibited a low onset overpotential of 76 mV and small overpotential of 120 mV at 10 mA cm^{-2} in an acidic electrolyte. Besides, it displayed a low Tafel slope of 53 mV dec^{-1}, a small interface charge transfer resistance, and long-time stability and durability, suggesting its remarkable properties as a promising HER electrocatalyst candidate.

Received 19th March 2020
Accepted 22nd April 2020

DOI: 10.1039/d0ra02530e

rsc.li/rsc-advances

1. Introduction

Sustainable energy development and increased environmental concerns have triggered imperative requirements for renewable and pollution-free new-generation energy sources.[1,2] As an energy carrier with entirely zero carbon composition and high energy density, hydrogen is regarded as one of the ideal clean alternatives to substitute traditional fossil fuels in the future.[3–5] The hydrogen evolution reaction (HER), a half-reaction occurring at the cathode during water electrolysis, can produce high purity hydrogen on a large scale in the industry. Owing to its renewability, theoretical feasibility and environmental benignity, HER has attracted increasing attention in recent decades. During the procedure of water electrolysis, the required theoretical voltage is 0 V for HER at 298 K.[6,7] However, extra electricity is demanded to overcome the overpotential caused by the activation energy barrier to kick start the initial reaction. Hence, high-efficient electrocatalysts are necessary to reduce the overpotential and accelerate reaction kinetics. At present, Pt-based materials with their onset overpotentials close to zero are recognized as the state-of-the-art electrocatalysts for HER.[8–10] Unfortunately, the rocketing cost, scarce reserve and mediocre stability of Pt-based materials seriously hinder their large-scale applications. Therefore, developing Pt-like, sustainable and cost-effective electrocatalysts remains a great challenge and urgent issue.

In the past years, a considerable number of Pt-free materials have emerged as HER electrocatalysts, including transition-metal sulfides, oxides, selenides, nitrides, phosphides, carbon-based materials and their compounds.[11–17] Among them, Ru-based materials are applied in various catalytic fields, such as hydrodesulfurization, electrocatalysis, photocatalysis, and supercapacitors.[18–24] Deriving from their rich redox chemistry and multiple valence states, Ru-based catalysts usually present exceptional electrocatalytic activities. RuS_2, one of the typical Ru-based materials, is usually used in hydrodesulfurization as an efficient catalyst.[25] Besides, subsequent explorations have proved that RuS_2 exhibits excellent HER activities.[26–28] In addition, the cost of Ru is less than 5% of metallic Pt, which is even more encouraging.[29,30] However, the previously reported electrocatalytic performance of RuS_2 for HER is still insufficient to meet the industrial needs. Therefore, extra efforts should be made to further improve the electrocatalytic efficiency of RuS_2.

Doping can modulate the electronic structure and narrow the bandgap, which is a commonly effective strategy to enhance the electrocatalytic performance of materials. A nitrogen (N) atom itself has a lone pair of electrons, strong electronegativity and small atomic radius. Therefore, N-doping can capture the electron around the metal atoms with weak electronegativity and affect the electronic density of the state of the material or

[a]*Physics and Electronic Engineering Department, Xinxiang University, Xinxiang 453003, P. R. China*

[b]*Key Laboratory of Sensor and Sensing Technology, Gansu Academy of Sciences, Lanzhou 730000, Gansu, China. E-mail: gao_xp02@163.com*

[c]*Key Laboratory for Magnetism and Magnetic Materials of MOE, Key Laboratory of Special Function Materials and Structure Design of MOE, Lanzhou University, Lanzhou 730000, P. R. China*

† Electronic supplementary information (ESI) available. See DOI: 10.1039/d0ra02530e

cause the distortion of the material phase structure by the atomic substitution.[31–33] Numerous experimental analysis as well as theoretical calculations revealed that the electronic conductivity and hydrogen adsorption capability of electrocatalysts are possible for notable improvements through N doping, enabling their implementation as an advanced cathode for HER.[34,35] Besides, designing multiphase structures can also improve the electrocatalytic efficiency owing to the usual formation of defects as well as exposed active sites at the atomic-scale interfaces.[36–38] A single atom of Ru has hydrogen adsorption properties similar to those of Pt since the bond strength of Ru–H is close to that of Pt–H, resulting in an outstanding electrocatalytic performance for the Ru catalyst.[39,40] Consequently, it is anticipated that RuS_2 embedded with a single atom of metallic Ru will exhibit a desirable HER activity.

Herein, we constructed a novel hybrid material, nitrogen-doped RuS_2 nanoparticles with *in situ* reduced Ru (N-RuS_2/Ru) as an electrocatalyst for HER. In order to introduce the nitrogen dopant, a pure RuS_2 was annealed at a low temperature in ammonia. Surprisingly, the obtained product is not only doped with nitrogen, but also has the appearance of an *in situ* reduced Ru metal phase, leading to a significantly improved electrocatalytic activity. Benefiting from the N dopant and reasonable designing of the interface between Ru and RuS_2, the electrocatalyst N-RuS_2/Ru displays optimal performance for HER in acid conditions far better than those of RuS_2 and RuS_2/Ru. In terms of experimental results, the as-synthesized N-RuS_2/Ru nanoparticles possess the lowest onset overpotential of 76 mV and a small Tafel slope of 53 mV dec^{-1}. The required overpotential is only 120 mV at a current density of 10 mA cm^{-2} in 0.5 M H_2SO_4. Moreover, it has long-term cycling stability.

2. Results and discussions

As shown in Fig. S1†, the pure RuS_2 was formed *via* subsequent sulfidation of Ru-based RuO_2 precursors (Fig. S2†) using a tube furnace. Next, the as-prepared RuS_2 was annealed in using ammonia to form the N-RuS_2/Ru product. For comparison, RuS_2/Ru was also prepared. The details of the experiments are described in the ESI.† The morphology and microstructure of the electrocatalysts were characterized *via* transmission electron microscopy (TEM) and scanning electron microscope (SEM). The SEM images of the samples shown in Fig. S3† indicate that the morphology of RuS_2, RuS_2/Ru and N-RuS_2/Ru

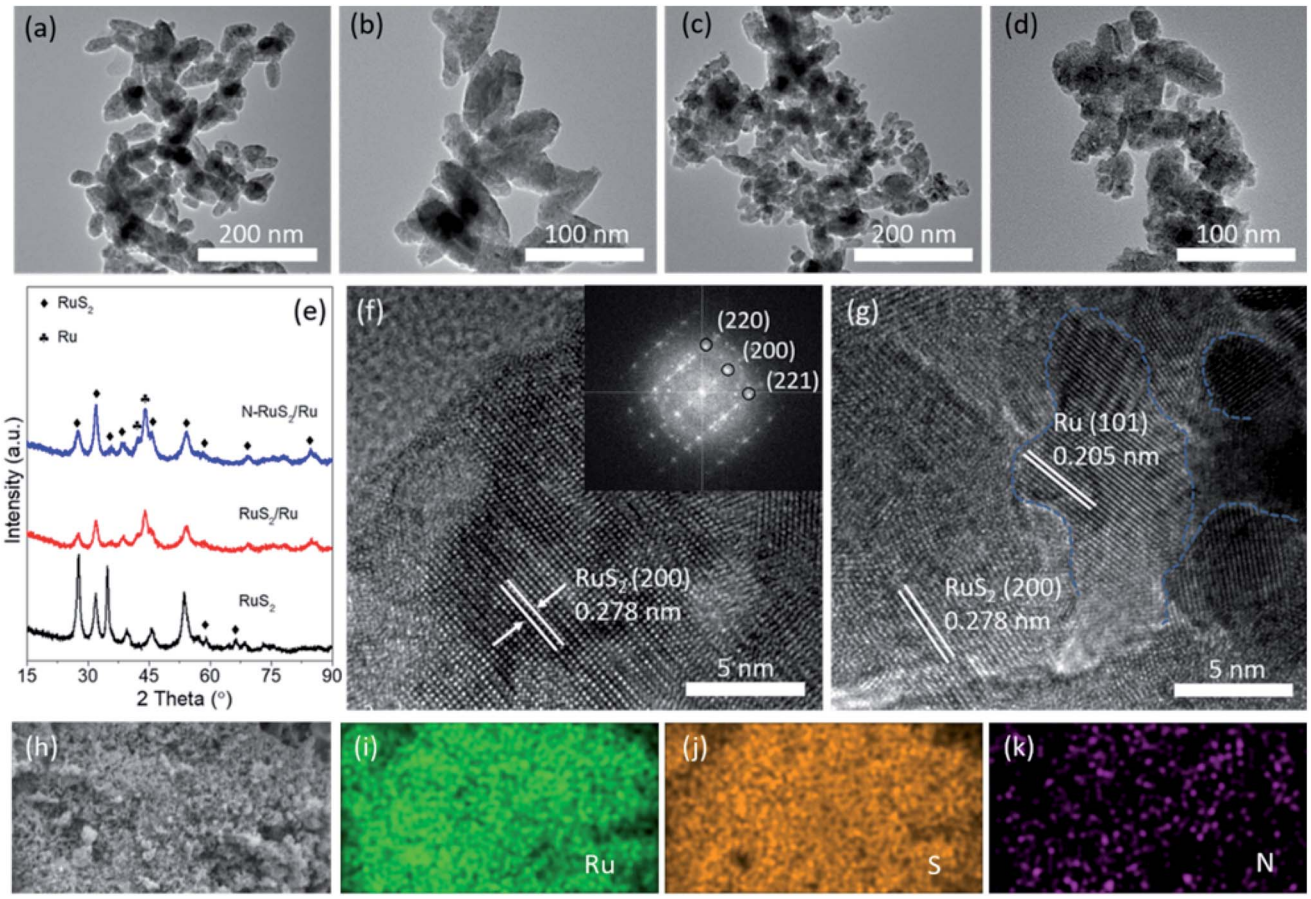

Fig. 1 (a) The low-magnification and (b) high-magnification TEM images of RuS_2. (c) The low-magnification and (d) high-magnification TEM images of N-RuS_2/Ru. (e) XRD spectra of RuS_2, RuS_2/Ru, and N-RuS_2/Ru. (f) High-resolution TEM image of RuS_2. The inset is the fast Fourier transform (FFT) of RuS_2. (g) High-resolution TEM image of the RuS_2 of N-RuS_2/Ru. (h–k) EDS mapping images of Ru, S, and N elements in N-RuS_2/Ru.

is an overlapped-nanoparticle type. Besides, we can see that RuS_2 is composed of scattered "wheat-like" nanoparticles with a diameter of about 50 nm (Fig. 1a and b). N-RuS_2/Ru shows the same morphology as that of pure RuS_2. It is worth mentioning that the particle size of N-RuS_2/Ru decreases slightly, and the surface becomes rougher (Fig. 1c and d), which is very gratifying as rough surfaces may expose more active sites for electrocatalytic reactions. Fig. 1e shows the X-ray diffraction (XRD) patterns of RuS_2, RuS_2/Ru and N-RuS_2/Ru. The pure RuS_2 shows a cubic structure with a crystal parameter of 0.561 nm, wherein three strongest peaks locate at 27.5°, 31.9° and 35.8° are indexed to the (111), (200) and (220) crystal planes, respectively. For RuS_2/Ru and N-RuS_2/Ru, in addition to the original diffraction peaks of RuS_2, different peaks of single metal Ru with the hexagonal structure were observed. The lattice fringes of RuS_2 and N-RuS_2/Ru were observed clearly in the high-resolution TEM images. The measured spacing of the lattice fringes for RuS_2 is 0.278 nm, corresponding to the (200) crystal face. In the fast Fourier transform (FFT) of RuS_2, the crystal planes corresponding to the diffraction points can be assigned to the (200), (220) and (221) planes, which is in good agreement with the XRD results. In the high-resolution TEM images of N-RuS_2/Ru, we also found the (101) crystal face of Ru metal with an interplanar distance of 0.205 nm besides the lattice fringes of RuS_2. Noting that the obvious crystal boundary can be observed between RuS_2 and Ru, which is likely in favor of the improvement of the catalytic activity. The energy-dispersive X-ray spectrum (EDS) mapping images (Fig. 1h–k) indicate that Ru, S, N are evenly and uniformly distributed in the whole selected region, confirming that the N element was incorporated into the samples.

The chemical states of RuS_2, RuS_2/Ru, and N-RuS_2/Ru were systematically explored *via* X-ray photoelectron spectroscopy (XPS), where the signals of S, Ru, and N in N-RuS_2/Ru were clearly observed. The S 2p spectrum of RuS_2 (Fig. 2a) shows two peaks centered at 162.7 eV and 163.9 eV, corresponding to the $2p_{3/2}$ and $2p_{1/2}$, respectively, which is consistent with the previous reports.[41] Note that the peak position of S 2p in RuS_2 and RuS_2/Ru shifts 0.3 eV to the higher binding energy. The possible reason is that the valence state of the surrounding sulfur atom is raised during the *in situ* Ru reduction process, while nitrogen doping has a trivial effect on the host anion. In Fig. 2b, the high-resolution Ru $3p_{3/2}$ spectra were magnified to check such subtle changes. The peak of Ru $3p_{3/2}$ in pure RuS_2 is located at 461.4 eV and is assigned to Ru^{4+}.[26] Due to the appearance of metallic Ru, Ru $3p_{3/2}$ of RuS_2/Ru naturally tends to the lower energy binding. After N-doping, some electrons of Ru around the dopant N are attracted by nitrogen with strong electronegativity, which enables the peak of Ru $3p_{3/2}$ in N-RuS_2/Ru shift back to the high binding energy. The high-resolution of the N 1s spectrum is presented in Fig. 2c. Two representative peaks located at 398.4 eV and 400.3 eV can be detected, which are contributed to chemisorbed N and doped N, respectively.[42] Furthermore, as shown in Fig. 2d, the results of the EDS spectrum illustrate that N-RuS_2/Ru contains Ru, S, N elements, and we can roughly estimate the nitrogen content as 6.67 at% (approximately equal to the result of XPS: 7.21 at%), and the ratio of Ru to S to N is 1 : 1.34 : 0.17. As a contrast, the EDS spectrum of RuS_2/Ru is provided in Fig. S4.† Comprehensively, the contribution of N in the EDS spectrum and N 1s in the high-resolution XPS spectrum as well as in the EDS mapping of N element in Fig. 1g consistently demonstrated that in addition to the single-phase Ru metal, the N element has also been successfully doped into RuS_2.

The electrocatalytic activities for HER of all the electrocatalysts were measured in an acidic medium (0.5 M H_2SO_4)

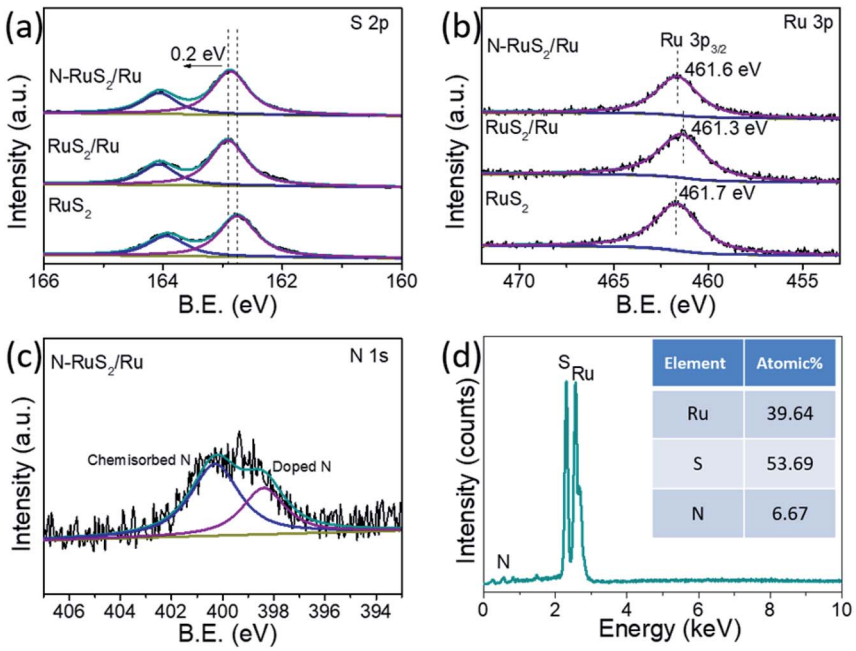

Fig. 2 High-resolution XPS spectra of (a) S 2p, (b) Ru 3p, and (c) N 1s. (d) EDS spectrum of N-RuS_2/Ru.

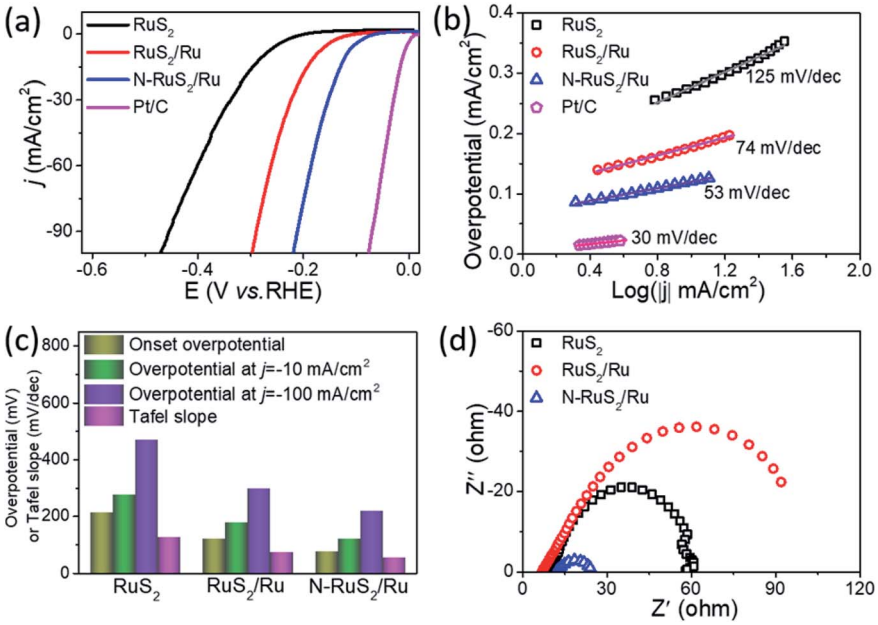

Fig. 3 (a) IR-corrected HER polarization curves of RuS_2, RuS_2/Ru, N-RuS_2/Ru and commercial Pt/C at a scan rate of 5 mV s^{-1} in 0.5 M H_2SO_4. (b) Tafel plots obtained from polarization curves *via* Tafel equation and (c) Overpotentials at different current densities of three samples and their Tafel slope. (d) EIS of RuS_2, RuS_2/Ru and N-RuS_2/Ru catalysts with a fixed overpotential of 150 mV.

using a typical three-electrode system. Commercial Pt/C was used as a benchmark sample for comparison under the same conditions. As shown in Fig. 3a, the polarization curves were first measured to analyze the HER activities of RuS_2, RuS_2/Ru and N-RuS_2/Ru nanoparticles electrocatalysts *via* the linear sweep voltammogram (LSV) methods. The onset overpotential, an important parameter of HER performance, can be known from the polarization curves. However, there are various methods to determine the value of the onset overpotential. For the sake of fairness, we chose the overpotential at the current density of 1 mA cm^{-2} as the onset overpotential. The results display that the N-RuS_2/Ru nanoparticles need a much lower onset potential of 76 mV to overcome the energy barrier of the initial reaction than do RuS_2 (~212 mV) and RuS_2/Ru (~121 mV) (Fig. 3a), which indicates that N-RuS_2/Ru has more reasonable hydrogen adsorption capacity and more efficient electrocatalytic active sites for HER. The satisfactory promotion is tremendously attributed to the interface effect of embedded-Ru with RuS_2, which leads to the formation of a large number of highly active reaction sites. Moreover, the defects and synergistic effect derived N-doping plays a vital role. To reach a current density of 10 mA cm^{-2}, a required overpotential is only 120 mV for the N-RuS_2/Ru nanoparticles, smaller than that of RuS_2/Ru (177 mV) and less than half of RuS_2 (276 mV). If we intend to continue to increase the current density to 100 mA cm^{-2}, the overpotential demand for N-RuS_2/Ru is 219 mV, while it is 297 mV for RuS_2/Ru, and 470 mV for RuS_2. To evaluate the HER kinetics of these electrocatalysts, their corresponding Tafel plots were further calculated and fitted based on the polarization curves, as shown in Fig. 3b. Obviously, compared with the pristine RuS_2 (125 mV dec^{-1}) and RuS_2/Ru (74 mV dec^{-1}), the N-RuS_2/Ru shows a much smaller Tafel slope of 53 mV dec^{-1}. Fig. 3c shows the overpotentials at different current densities for three samples and corresponding Tafel slopes, their electrocatalytic activities can be seen and compared at a glance. These results are comparable or superior to those recently reported on representative HER electrocatalysts (Table S1, ESI†). Electrochemical impedance spectra (EIS) of the three electrocatalysts were obtained by the AC electrochemistry impendence test. A smaller impedance arc radius relates a lower interface charge transfer resistance (R_{ct}), *i.e.*, a faster reaction rate.[7,17] It can be seen in Fig. 3d that N-RuS_2/Ru has a minimum impedance arc radius among three samples, indicating its outstanding interface transfer conductivity. The ahead analysis results confirm that N-doping has modulated the electron density of RuS_2, and the *in situ* reduced Ru also affected the electronic state of catalysts. Changes in R_{ct} demonstrate that N-doping and embedded-Ru have successfully promoted the interface electron transfer rate of RuS_2 in the reaction process.

Fig. 4a shows the CV curves of N-RuS_2/Ru, which were collected at −0.2 to 0 V (*vs.* Ag/AgCl) under a series of scan rates ranged from 20 to 100 mV s^{-1} *via* cyclic voltammetry. The CV curves of RuS_2 and RuS_2/Ru have been provided in Fig. S5 in ESI.† Next, half of the differences in current density variation ($\Delta j/2 = (j_a - j_c)/2$) at a certain potential of −0.1 V (*vs.* Ag/AgCl) were plotted against the scan rate, as shown in Fig. 4b. The electrochemical double-layer capacitance (C_{dl}) can be estimated by the linear fitting. N-RuS_2/Ru exhibits the largest C_{dl} of 41 mF cm^{-2}, more than twice that of RuS_2 (16 mF cm^{-2}). The largest value of C_{dl} indicates that N-RuS_2/Ru has the largest electrochemically active surface area (ECSA) because C_{dl} is considered to be directly related to ECSA.[43,44] In addition, N-RuS_2/Ru also displays the best turn over frequency (TOF) (2.115 s^{-1} at an overpotential of 200 mV) among the three electrocatalysts

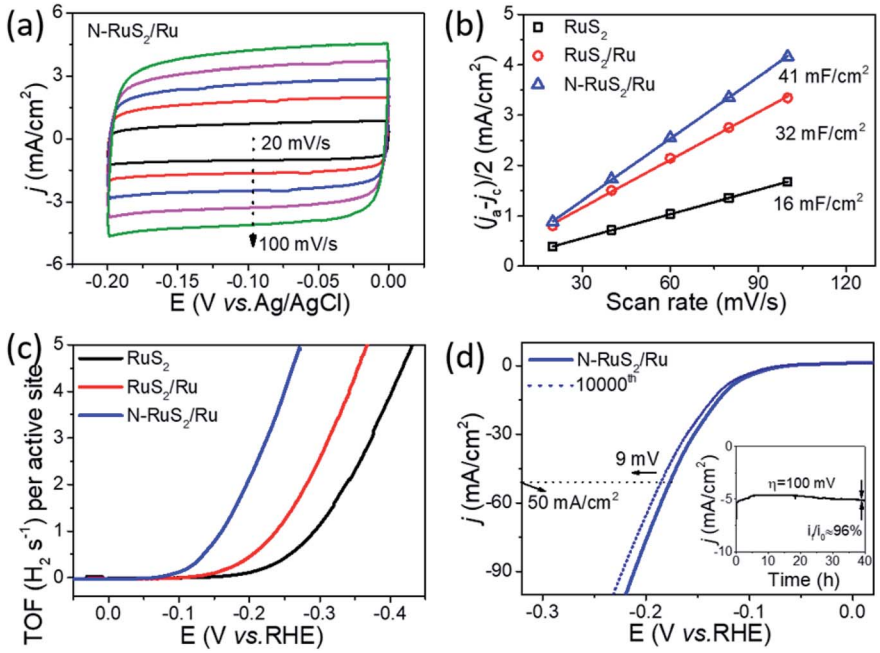

Fig. 4 (a) CV scans of the double-layer capacitance measurement of N-RuS_2/Ru at different scanning rates. (b) Double-layer capacitances of RuS_2, RuS_2/Ru and N-RuS_2/Ru catalysts. (c) TOF curves of all samples against the HER potentials. (d) Polarization curves of N-RuS_2/Ru before and after 10 000 CV cycles from −0.2 to 0 V (*vs.* RHE) (inset: chronoamperometry curves tested at a fixed overpotential of 100 mV for 40 h).

(Fig. 4c). Under the equal overpotential, the TOF values of RuS_2 and RuS_2/Ru are 0.107 s^{-1} and 0.438 s^{-1}, respectively, which are far lower than that of N-RuS_2/Ru. To reach 0.725 s^{-1} of TOF as Pt,[45] N-RuS_2/Ru requires an overpotential of 147 mV, much smaller than those of RuS_2 (276 mV) and RuS_2/Ru (221 mV). This data further confirms the superior HER performances of N-RuS_2/Ru. Both the results of ECSA and TOF suggest that N-RuS_2/Ru has higher electrocatalytic activity toward HER. The electrocatalytic parameters of the three electrocatalysts are listed in Table S2.† Except for the electrocatalytic activity, the durability of N-RuS_2/Ru is also evaluated under a long-term cycling test. As shown in Fig. 4d, the overpotential at a current density of 50 mA cm^{-2} for N-RuS_2/Ru nanoparticles has a slight increase of only 9 mV, better than those of RuS_2 (+26 mV) and RuS_2/Ru (+16 mV) (Fig. S6†). Besides, the current density is reduced by only 4% after a constant chronoamperometry (overpotential: 100 mV) test for 40 h, further illustrating the excellent stability of N-RuS_2/Ru nanoparticles. It is worth mentioning that the micromorphology of N-RuS_2/Ru nanoparticles is basically retained after the cycling test (Fig. S7†).

The enhancement of the catalytic activity of N-RuS_2/Ru is mainly due to the combination of nitrogen doping and the *in situ* reduction Ru metal as well as the synergistic effect. Doping nitrogen can adjust the electronic structure, narrow the bandgap of the semiconductor catalysts RuS_2, accelerate the surface electronic transfer and activate the surrounding atoms (such as Ru or S) as the efficient active sites, which will lead to an increase in active sites.[46,47] Moreover, the introduction of nitrogen may result in some defects in the structures, which will be of great benefit to the improvement of catalytic efficiency. In addition, Ru, as a precious metal, has similar hydrogen adsorption capacity to Pt, indicating the presence of extremely efficient active sites.[39,40] Meanwhile, it forms an atomic-scale interface structure with RuS_2. We know that interface engineering is a critical and effective route to expand the catalytic activity.[48–50] The electronic states near the interface will be optimized, and the chemical states of atoms near the interface will also be affected, which will eventually promote a rapid electron transfer and appropriate hydrogen adsorption in HER.

3. Conclusions

In summary, we have successfully prepared N-RuS_2/Ru nanoparticles used as an efficient electrocatalyst for HER. Reasonable design and simplified synthesis strategy produced a cost-effective and high-performance electrocatalyst. N-doping can optimize the electronic structure to enhance the conductivity of N-RuS_2/Ru. The *in situ* reduced Ru metal phase increases the atomic-scale interface in the materials, which is particularly conducive to the promotion of the electrocatalytic activity. Thus, the as-synthesized N-RuS_2/Ru exhibits a remarkable performance for HER in 0.5 M H_2SO_4. It presents the lowest onset overpotential of 76 mV, a required overpotential of 120 mV and 219 mV at the current density of 10 mA cm^{-2} and 100 mA cm^{-2}, respectively. The N-RuS_2/Ru electrocatalyst also has a small Tafel slope of 53 mV dec^{-1} and a large electrochemically active surface area. The turnover frequency of N-RuS_2/Ru is high up to 2.115H_2 s^{-1} at an overpotential of 200 mV. Moreover, it has long-term stability over 10 000 cycles. This work paves a new avenue to design robust Pt-free electrocatalysts for hydrogen production toward commercial water electrolysis.

Conflicts of interest

The authors declare that they have no conflict of interest.

Acknowledgements

This work is supported by the Science Fund of Educational Department of Henan Province of China and the Ninth Group of Key Disciplines in Henan Province (grant no. 2018119). It is also supported by the Application Research and Development Plan of Gansu Academy of Sciences (2018JK-16), Key Research and Development Plan of Gansu Province (No. 18YF1GA088) and Innovative Team Construction Project of Gansu Academy of Science (2020CX005-01).

References

1 A. J. Bard and M. A. Fox, *Acc. Chem. Res.*, 1995, **28**, 141.
2 J. Chow, R. J. Kopp and P. R. Portney, *Science*, 2003, **302**, 1528.
3 X. Zou and Y. Zhang, *Chem. Soc. Rev.*, 2015, **44**, 5148.
4 N. Armaroli and V. Balzani, *Angew. Chem., Int. Ed.*, 2007, **46**, 52–66.
5 H. W. Liang, S. Brüller, R. Dong, J. Zhang, X. Feng and K. Müllen, *Nat. Commun.*, 2015, **6**, 7992.
6 S. P. S. Badwal, S. S. Giddey, C. Munnings, A. I. Bhatt and A. F. Hollenkamp, *Front. Chem.*, 2014, **2**, 79.
7 J. Wang, F. Xu, H. Jin, Y. Chen and Y. Wang, *Adv. Mater.*, 2017, 1605838.
8 R. Subbaraman, D. Tripkovic, D. Strmcnik, K. C. Chang, M. Uchimura, A. P. Paulikas, V. tamenkovic and N. M. Markovic, *Science*, 2011, **334**, 1256.
9 D. V. Esposito, S. T. Hunt, Y. C. Kimmel and J. G. G. Chen, *J. Am. Chem. Soc.*, 2012, **134**, 3025.
10 J. Greeley, T. F. Jaramillo, J. Bonde, I. B. Chorkendorff and J. K. Norskov, *Nat. Mater.*, 2006, **5**, 909.
11 Y. G. Li, H. L. Wang, L. M. Xie, Y. Y. Liang, G. S. Hong and H. J. Dai, *J. Am. Chem. Soc.*, 2011, **133**, 7296.
12 W. B. Lu, T. T. Liu, L. S. Xie, C. Tang, D. N. Liu, S. Hao, F. L. Qu, G. Du, Y. J. Ma, A. M. Asiri and X. P. Sun, *Small*, 2017, **13**, 1700805.
13 S. J. Deng, F. Yang, Q. H. Zhang, Y. Zhong, Y. X. Zeng, S. W. Lin, X. L. Wang, X. H. Lu, C. Z. Wang, L. Gu, X. H. Xia and J. P. Tu, *Adv. Mater.*, 2018, **30**, 1802223.
14 Z. Y. Chen, Y. Song, J. Y. Cai, X. S. Zheng, D. D. Han, Y. S. Wu, Y. P. Zang, S. W. Niu, Y. Liu, J. F. Zhu, X. J. Liu and G. M. Wang, *Angew. Chem., Int. Ed.*, 2018, **57**, 5076.
15 Q. Liu, J. Q. Tian, W. Cui, P. Jiang, N. Y. Cheng, A. M. Asiri and X. P. Sun, *Angew. Chem., Int. Ed.*, 2014, **53**, 6710.
16 Y. P. Liu, G. T. Yu, G. D. Li, Y. H. Sun, T. Asefa, W. Chen and X. X. Zou, *Angew. Chem., Int. Ed.*, 2015, **54**, 10752.
17 I. K. Mishra, H. Zhou, J. Sun, K. Dahal, S. Chen and Z. Ren, *Energy Environ. Sci.*, 2018, 1.
18 E. J. Popczun, J. R. McKone, C. G. Read, A. J. Biacchi, A. M. Wiltrout, N. S. Lewis and R. E. Schaak, *J. Am. Chem. Soc.*, 2013, **135**, 9267.
19 E. J. Popczun, C. G. Read, C. W. Roske, N. S. Lewis and R. E. Schaak, *Angew. Chem., Int. Ed.*, 2014, **53**, 5427.
20 W. Cui, Q. Liu, Z. Xing, A. M. Asiri, K. A. Alamry and X. Sun, *Appl. Catal., B*, 2015, **164**, 144.
21 Z. Pu, I. S. Amiinu, Z. Kou, W. Li and S. Mu, *Angew. Chem., Int. Ed.*, 2017, **56**, 11559.
22 A. P. Gaikwad, D. Tyagi, C. A. Betty and R. Sasikala, *Appl. Catal., A*, 2016, **517**, 91.
23 B. S. Lou, P. Veerakumar, S. M. Chen, V. Veeramani, R. Madhu and S. B. Liu, *Sci. Rep.*, 2016, **6**, 19949.
24 P. R. Deshmukh, S. N. Pusawale, A. D. Jagadale and C. D. Lokhande, *J. Mater. Sci.*, 2012, **47**, 1546.
25 M. Lacroix, N. Boutarfa, C. Guillard, M. Vrinat and M. Breysse, *J. Catal.*, 1989, **120**, 473.
26 J. Yu, Y. Guo, S. Miao, M. Ni, W. Zhou and Z. Shao, *ACS Appl. Mater. Interfaces*, 2018, **10**, 34098.
27 M. Cheng, H. Geng, Y. Yang, Y. Zhang and C. C. Li, *Chem.–Eur. J.*, 2019, **25**, 8579.
28 J. Q. Chi, X. J. Zeng, X. Shang, B. Dong, Y. M. Chai, C. G. Liu, M. Marin and Y. Yin, *Adv. Funct. Mater.*, 2019, 1901790.
29 Y. Zheng, Y. Jiao, Y. Zhu, L. Li, Y. Han, Y. Chen, M. Jaroniec and S. Qiao, *J. Am. Chem. Soc.*, 2016, **138**, 16174.
30 J. Mahmood, F. Li, S. Jung, M. S. Okyay, I. Ahmad, S. Kim, N. Park, H. Y. Jeong and J. B. Baek, *Nat. Nanotechnol.*, 2017, **12**, 441.
31 S. Chen and S. Z. Qiao, *ACS Nano*, 2013, **7**, 10190.
32 A. Aijaz, J. Masa, C. Rosler, W. Xia, P. Weide, A. J. Botz, R. A. Fischer, W. Schuhmann and M. Muhler, *Angew. Chem., Int. Ed.*, 2016, **55**, 4087.
33 J. Zhang, T. Wang, D. Xue, C. Guan, P. Xi, D. Gao and W. Huang, *Energy Storage Mater.*, 2020, **25**, 202.
34 M. Yu, Z. Wang, C. Hou, Z. Wang, C. Liang, C. Zhao, Y. Tong, X. Lu and S. Yang, *Adv. Mater.*, 2017, 1602868.
35 D. Hou, W. Zhou, K. Zhou, Y. Zhou, J. Zhong, L. Yang, J. Lu, G. Li and S. Chen, *J. Mater. Chem. A*, 2015, **3**, 15962.
36 Y. Liu, C. Ma, Q. Zhang, W. Wang, P. Pan, L. Gu, D. Xu, J. Bao and Z. Dai, *Adv. Mater.*, 2019, **31**, 1900062.
37 Q. Liang, L. Zhong, C. Du, Y. Luo, J. Zhao, Y. Zheng, J. Xu, J. Ma, C. Liu, S. Li and Q. Yan, *ACS Nano*, 2019, **13**, 7975.
38 P. Liu, J. Ran, B. Xia, S. Xi, D. Gao and J. Wang, *Nano-Micro Lett.*, 2020, **12**, 68.
39 Y. Zheng, Y. Jiao, Y. H. Zhu, L. H. Li, Y. Han, Y. Chen, M. Jaroniec and S. Z. Qiao, *J. Am. Chem. Soc.*, 2016, **138**, 16174.
40 J. Wang, Z. Z. Wei, S. J. Mao, H. R. Li and Y. Wang, *Energy Environ. Sci.*, 2018, **11**, 800.
41 K. Krishnamoorthy, P. Pazhamalai and S. J. Kim, *Electrochim. Acta*, 2017, **227**, 85.
42 M. Yu, Z. Wang, C. Hou, Z. Wang, C. Liang, C. Zhao, Y. Tong, X. Lu and S. Yang, *Adv. Mater.*, 2017, **29**, 1602868.
43 I. K. Mishra, H. Q. Zhou, J. Y. Sun, K. Dahal, Z. S. Ren, R. He, S. Chen and Z. F. Ren, *Mater. Today Phys.*, 2018, **4**, 1.
44 H. Q. Zhou, F. Yu, Y. F. Huang, J. Y. Sun, Z. Zhu, R. J. Nielsen, R. He, J. M. Bao, W. A. Goddard III, S. Chen and Z. F. Ren, *Nat. Commun.*, 2016, **7**, 12765.
45 T. F. Jaramillo, K. P. Jørgensen, J. Bonde, J. H. Nielsen, S. Horch and I. Chorkendorff, *Science*, 2007, **317**, 100.

46 J. Jiang, F. Sun, S. Zhou, W. Hu, H. Zhang, J. Dong, Z. Jiang, J. Zhao, J. Li, W. Yan and M. Wang, *Nat. Commun.*, 2018, **9**, 2885.
47 S. H. Ye, Z. X. Shi, J. X. Feng, Y. X. Tong and G. R. Li, *Angew. Chem., Int. Ed.*, 2018, **57**, 2672.
48 Y. Wu, F. Li, W. Chen, Q. Xiang, Y. Ma, H. Zhu, P. Tao, C. Song, W. Shang, T. Deng and J. Wu, *Adv. Mater.*, 2018, **30**, 1803151.
49 J. Yin, Y. Li, F. Lv, Q. Fan, Y.-Q. Zhao, Q. Zhang, W. Wang, F. Cheng, P. Xi and S. Guo, *ACS Nano*, 2017, **11**, 2275.
50 J. Yin, Y. Li, F. Lv, M. Lu, K. Sun, W. Wang, L. Wang, F. Cheng, Y. Li, P. Xi and S. Guo, *Adv. Mater.*, 2017, **29**, 1704681.